Laser synthesis and functionalization of nanostructures

OPEN ACCESS
IOP Publishing | IMMT
International Journal of Extreme Manufacturing
Int. J. Extrem. Manuf. 1 (2019) 012002 (13pp)
https://doi.org/10.1088/2631-7990/ab0eca

Topical Review

Laser synthesis and functionalization of nanostructures

Costas P Grigoropoulos

Laser Thermal Laboratory, Department of Mechanical Engineering, University of California at Berkeley, 6129 Etcheverry Hall, Berkeley CA 94720-1740, United States of America

E-mail: cgrigoro@berkeley.edu

Received 12 March 2019
Accepted for publication 12 March 2019
Published 10 April 2019

Abstract

This article summarizes work at the Laser Thermal Laboratory and discusses related studies on the laser synthesis and functionalization of semiconductor nanostructures and two-dimensional (2D) semiconductor materials. Research has been carried out on the laser-induced crystallization of thin films and nanostructures. The *in situ* transmission electron microscopy (TEM) monitoring of the crystallization of amorphous precursors in nanodomains is discussed herein. The directed assembly of silicon nanoparticles and the modulation of their optical properties by phase switching is presented. The vapor–liquid–solid mechanism has been adopted as a bottom-up approach in the synthesis of semiconducting nanowires (NWs). In contrast to furnace heating methods, laser irradiation offers high spatial selectivity and precise control of the heating mechanism in the time domain. These attributes enabled the investigation of NW nucleation and the early stage of nanostructure growth. Site- and shape-selective, on-demand direct integration of oriented NWs was accomplished. Growth of discrete silicon NWs with nanoscale location selectivity by employing near-field laser illumination is also reported herein. Tuning the properties of 2D transition metal dichalcogenides (TMDCs) by modulating the free carrier type, density, and composition can offer an exciting new pathway to various practical nanoscale electronics. *In situ* Raman probing of laser-induced processing of TMDC flakes was conducted in a TEM instrument.

Keywords: laser nanofabrication, laser crystallization, nanowire growth, near field scanning optical microscopy, transition metal dichalcogenides

(Some figures may appear in colour only in the online journal)

1. Nanoscale melting and crystallization

1.1. In situ observation experiments

Laser-based processing enables a wide variety of device configurations comprised of thin films and nanostructures on sensitive and even flexible substrates which are not possible with traditional thermal annealing schemes [1]. The crystallization of amorphous thin films is a critical fabrication step for enhancing the performance of thin-film transistors [2, 3] and thin-film solar cell devices [4]. Typical thin-film materials offer cost-effective device fabrication routes but intrinsically suffer from a low degree of crystallinity and hence require improvements by subsequent thermal annealing. Using a furnace to increase crystallinity not only requires a large thermal budget but also limits the adoption of inexpensive substrates, such as pyrex, soda-lime glass, or polymer substrates [5]. Annealing by pulsed lasers can significantly mitigate these issues by taking advantage of precisely localized heating [6]. Laser-induced crystallization is a promising

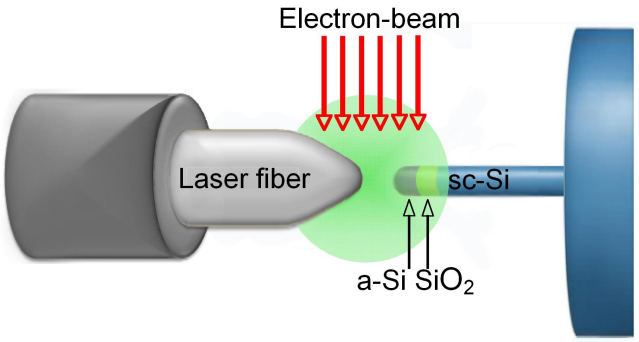

Figure 1. Schematic of the *in situ* TEM optical near-field setup [14]. In this experiment, 532 nm laser irradiation is delivered through the probe. Reprinted with permission from [14]. Copyright (2012) American Chemical Society.

tool for realizing melt-mediated growth of crystalline silicon (Si). However, the localized heat-affected area can suffer rapid heat loss; and the subsequent severe undercooling can instigate numerous nucleation events. Accordingly, the crystallization process can end up with a myriad of crystalline grains, i.e. polycrystalline silicon (pc-Si). When un-melted crystallites exist in the initial stage of crystallization, these seeds also provide active growth sites, leading to crystallization into pc-Si. However, the pc-Si grain boundaries degrade the electronic performance. These issues have motivated development of various crystallization techniques (including superlateral growth [2], grain filter [7, 8], and crystal-seeded growth [9]) to enlarge the grain size and reduce the density of grain boundaries.

Researchers have reported on the synthesis of one-dimensional (1D) nanostructures in electron microscopy instruments by far-field optics [10, 11]. It has been demonstrated that laser-induced nanoscale melting of amorphous silicon (a-Si) can effectively lead to the formation of single-crystalline nanodomains after re-solidification on single-crystal Si substrates [12, 13]. An *in situ* transmission electron microscope (TEM) monitoring technique was implemented to observe the crystallization of a-Si during laser irradiation by directly coupling a laser beam into a TEM using a fiber optic probe [14, 15]. In contrast to prior *in situ* TEM observations of laser-induced phase transformations [16, 17], this approach uses a near-field technique.

Figure 1 shows a schematic of a near-field scanning optical microscopy (NSOM) probe coupled into a TEM. The fiber probe tip is precisely positioned to illuminate a-Si precursors prepared by focused ion beam (FIB) processing. Figure 2 shows the results from laser-induced crystallization of an a-Si pillar structure with a nanosecond (ns) laser where the entire sample width is within the spot size of the laser. Progressing from a-Si (figure 2(a)) to pc-Si (figure 2(b)) to a final cap of single-crystal Si (sc-Si) (figures 2(c) and (d)).

The transient temperature evolution during crystallization has a critical influence on the resulting microstructure [18–20]. In order to gain insight into the crystallization of a single-crystal Si cap, a 3D transient heat transfer simulation combined the classical homogeneous and heterogeneous nucleation mechanisms [21], based on the finite difference method [19, 20, 22]. Heterogeneous nucleation prevails over the homogeneous mechanism at a relatively higher temperature, not allowing deeper undercooling. Quasi-steady state (QSS) estimates of the nucleation rate were assumed in the simulation. More elaborate nucleation kinetics, such as athermal [23, 24] and non-QSS [24] nucleation, may emerge during the relatively fast cooling rate. However, several theoretical papers confirm that the calculated cooling rate ($\sim 7 \times 10^9$ K s^{-1}) is in the QSS regime (or moderately close to QSS [23]). The simulations showed that the nucleation commenced at a temperature of 1240–1330 K. The nucleation rate dramatically increased with the degree of undercooling. Hence, growth of single crystal happened when the recalescence due to the latent heat release was sufficient to quench subsequent nucleation events.

Massively parallel lithography techniques (possibly nanoimprint lithography or e-beam lithography) could be configured to fabricate the base structures. Subsequent laser crystallization steps would form nanoscale crystalline dot arrays to serve as controlled seeds for polycrystalline or even epitaxial film growth by chemical vapor deposition (CVD) [25]. Such an approach could lead to polycrystalline films with tailored grain distribution.

Experiments on the crystallization of long a-Si nanopillars were performed on the same TEM-based setup discussed above [26]. In this case, Si nanopillars (diameter: 300–400 nm, length: 1.7–2 μm) consisting of a-Si—silicon oxide ($\sim$100 nm)—crystalline Si layers were fabricated by an FIB technique. In contrast to the previously discussed study where a confined a-Si fully melted, the laser heat could only affect the phase of the pillar extremity. As shown in figure 3, the initial a-Si pillar was crystallized into pc-Si but with an unusually large sc-Si grain at the tip. Electron diffraction patterns confirmed single crystallinity of the large tip grain. The confined lateral (or radial) dimension prevented additional grains from growing into columnar structures [27]. Moreover, growth of the diverging secondary grains was preferentially frustrated by lateral confinement. The formation of the large tip crystal is reminiscent of the argument of Im *et al* [2] on the formation of large sc-Si from a-Si thin films and also of a study by Leung *et al* [27]. Large-area laser irradiation, including expanded/homogenized beam scanning, could incur efficient crystallization of pillar arrays. The resulting pillar arrays and the exposed single-crystalline surface may serve as a growth template and crystalline seeds for the controlled growth of sc-Si.

1.2. Assembly and phase switching of silicon nanoparticles (NPs)

Patterned periodic nanostructures serve as building blocks in electronics [28], spintronics [29], chemical catalysts [30], plasmonic and photonic devices [31–33], and memory devices [34–36]. Various efforts have been made to write nanostructures into well-defined configurations. Electron-beam lithography and helium-FIB processing represent ultrahigh resolution, top-down approaches. On the other hand,

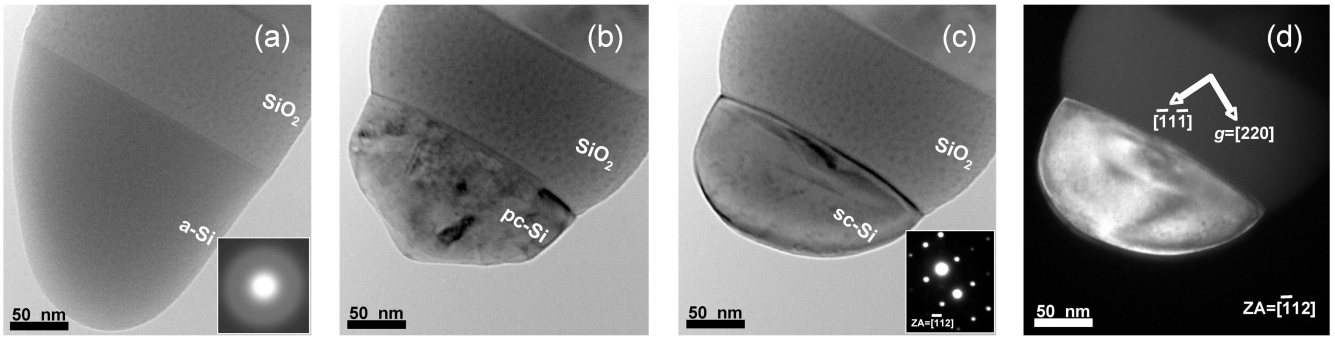

Figure 2. (a) As-prepared nanoscale a-Si pillar fabricated by FIB. (b) TEM image of pc-Si observed after irradiation by several ns laser pulse shots. (c) Bright-field TEM image of single-crystalline, nanoscale sc-Si cap achieved after the pc-Si cap shown in (b) irradiated by a single-pulse shot of ns laser beam. Inset: electron diffraction pattern of the nanoscale sc-Si as shown in (c), zone axis is [−112]. (d) The corresponding dark-field TEM image of the nanoscale sc-Si grain as shown in (c), using the [220] reflection to illuminate only the lone Si grain. Reprinted with permission from [14]. Copyright (2012) American Chemical Society.

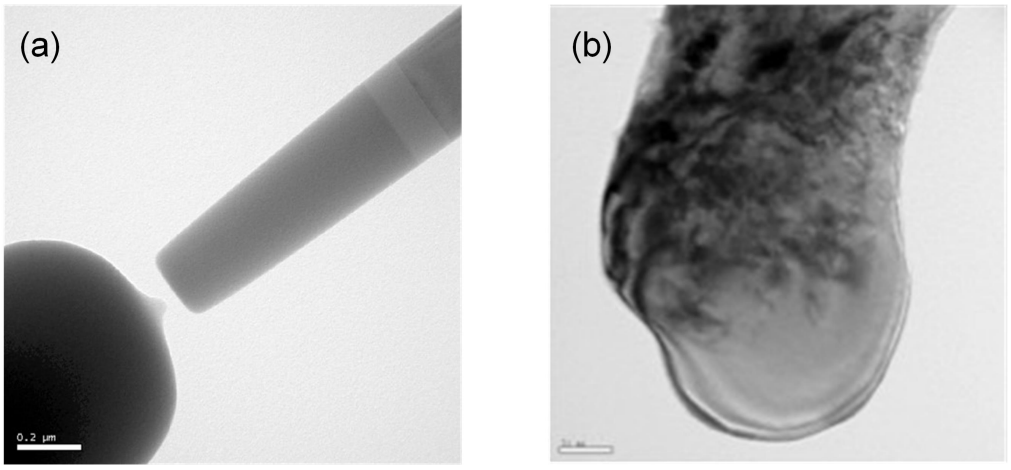

Figure 3. The figure (a) shows the NSOM probe against an a-Si pillar. The figure (b) shows the crystal structure obtained upon irradiation of laser pulses. Reproduced from [26] (2014). With permission of Springer.

bottom-up, self-assembly relies on fundamental chemical processes offering a scalable nanomanufacturing path. Pattern-guided laser [37–39] and thermal [40, 41] dewetting, as well as liquid assembly [42, 43], can produce periodic metallic and dielectric nanostructures combining pattern fidelity and low cost. Advancements in structural color [44–48], optical data storage [49, 50], and active nanophotonic devices [51–53] rely on tuning of the patterned geometrical features. Optical field patterning is a promising route [54–56]. The laser-induced forward transfer (LIFT) method has been employed to print Si resonators with tunable size [57].

A laser-based method that can tune the size, number, symmetry, and crystallinity of Si NP arrays was recently reported [58]. Laser-induced modulated assembly utilizes nanosecond laser pulse irradiation as a source modulating the assembly of a prepatterned a-Si film to a periodic NP array (figures 4(a) and (b)) The LiMA process relies on modulation of the local laser absorption due to the near-field optical energy coupling. Due to the near-field interaction, LiMA does not require elaborate focusing of the laser beam and is easily scalable. The modulation entails polarization-dependent particle sizing, fluence-dependent particle number selection, and deliberate particle subtraction. Amorphization of crystalline Si NPs follows via laser-induced phase switching (LiPS), due to the fast cooling rate upon nanosecond irradiation. Phase switching has usually been observed in compound phase change materials, such as germanium antimony tellurium (GeSbTe). The ensuing structural modification leads to dielectric constant switching.

In Wang *et al*'s study, LiMA and LiPS could program the Si Mie resonator combination as well as the resonance peak position and the dielectric constant of selected resonators in three different scales. The complex NP arrangement modulated by the laser pulse energy and polarization produced particle sizes ranging from 60 to 330 nm. The number of Mie resonators as well as the resonance peaks and dielectric constants of selected resonators can be programmed. Optical metasurfaces [59], structural color, and multidimensional optical storage devices could be fabricated using this approach. Dielectric NPs exhibit a significant advantage over plasmonics due to low loss and compatibility with conventional semiconductor processing and manufacturing. The present method can ultimately produce monoperiodic, biperiodic and triperiodic patterns, directly facilitating the

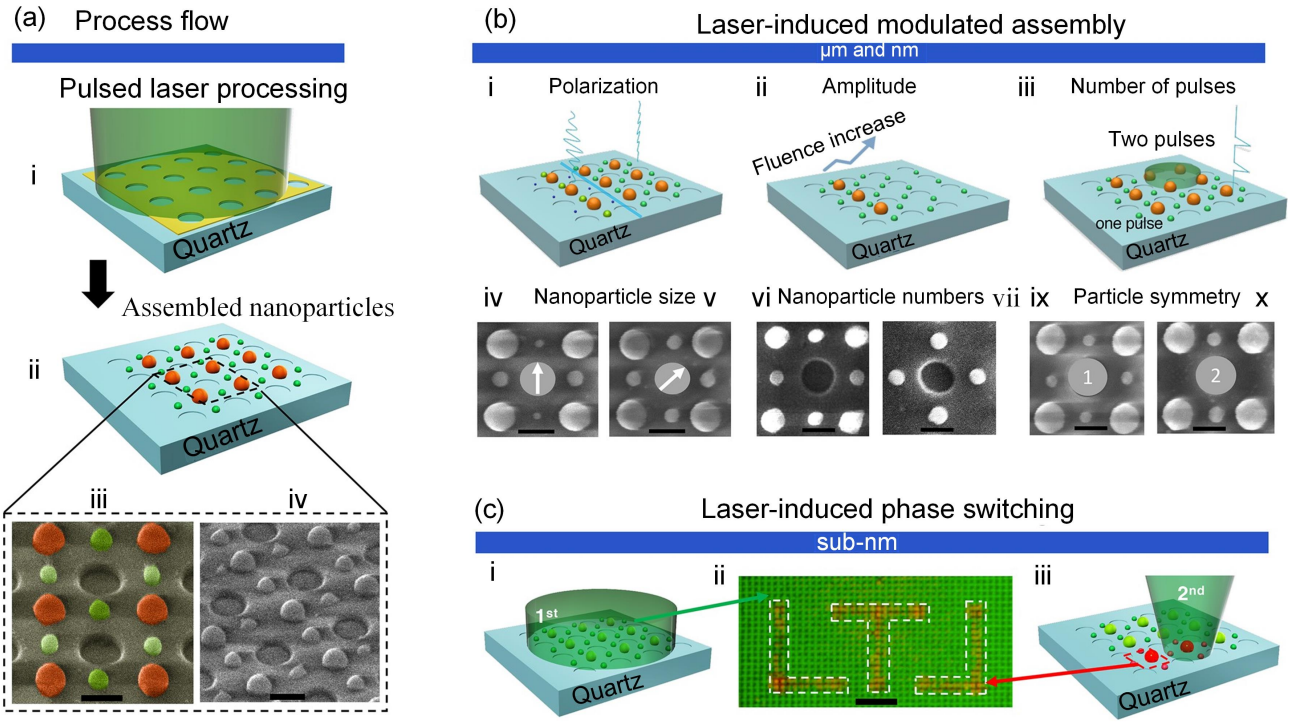

Figure 4. (a) Schematics of the LIMA nanoparticle assembly process flow and SEM images of assembled nanoparticle arrays. (b) LiMA results using different laser processing parameters. (c) LiPS of Si nanoparticle crystallinity and its effect on color appearance. A second pulse changed the color of a preassembled nanoparticle canvas through from 'green' to 'red' through amorphization of crystalline Si. The scale bars are 300 nm for (a) (iii)–(iv) and (b) (iv)–(iv) and 5 μm for (c) (ii). Reprinted with permission from [58]. Copyright (2018) American Chemical Society.

application of Fano resonance [60, 61] and spectroscopy [62]. In a broader context, the concept of Si as 'phase change' material may find applications in storage and reconfigurable metasurfaces.

2. Directed laser nanomaterial growth

2.1. Laser-aided vapor–liquid–solid (VLS) nanowire (NW) growth

Nanoscale-synthesized materials are the key to building future generation devices in diverse fields, including NW-based applications in energy conversion [63, 64], energy storage [65, 66], optoelectronics [67, 68], and biotechnology [69, 70]. To realize this promise, new techniques must be developed to enable the precise layout and assembly of heterogeneous components into functional 'superblocks.' Even though a high level of compositional and orientational control in NW growth has been achieved, the post-synthesis assembly steps, even by state-of-the-art optical or optoelectronic tweezing [71, 72], are not sufficient to allow high spatial and directional precision. As a route towards this goal, several studies have attempted site-selective growth of NWs [73, 74] or nanotubes [75, 76] by local laser illumination. Laser-assisted NW (nanotube) growth broadly falls into the category of laser CVD which has been actively explored for a few decades [77] as a versatile materials synthesis technique enabling the formation of microstructures of well-defined dimensions in a single-step maskless process [78].

The VLS crystal growth approach is utilized for the fabrication of high aspect ratio nanoscale semiconductor materials. In the VLS mechanism, the gold (Au) catalyst forms a liquid alloy with Si that preferentially adsorbs onto the catalyst surface at the eutectic temperature of 363 °C or higher and then diffuses into the Au–Si liquid alloy droplet. After reaching the solubility limit at the liquid–solid interface, Si precipitates inducing NW growth. Actual growth begins after an elapsed time, typically called the *nucleation time* (or *incubation time*). The shortest nucleation time reported was in the range of 15 s at 650 °C growth temperature (for an ~30 nm diameter Au catalyst) and extended to ~180 s at 450 °C [79]. Considering that the possible contributing factors to this elapsed time are reaction and diffusion, mediated by phase change of the silicon species through molten catalyst of only tens of nm in diameter, these times appear to be too long.

The laser-assisted growth mechanism of silicon nanowires (SiNWs) has been investigated via the heating of deposited catalysts [80]. Figure 5 shows vertical growth of SiNWs on a homoepitaxial c-Si film. The heterogeneity in length that is controlled by the laser duration is notable. Conductive heat transfer analysis shows that the induced, nearly steady, temperature in the time regime of seconds exhibits a linear relationship with respect to the laser power applied. The NW growth follows typical Arrhenius behavior with an activation energy of ~66.8 (kcal mol^{-1}). Laser-assisted multielement

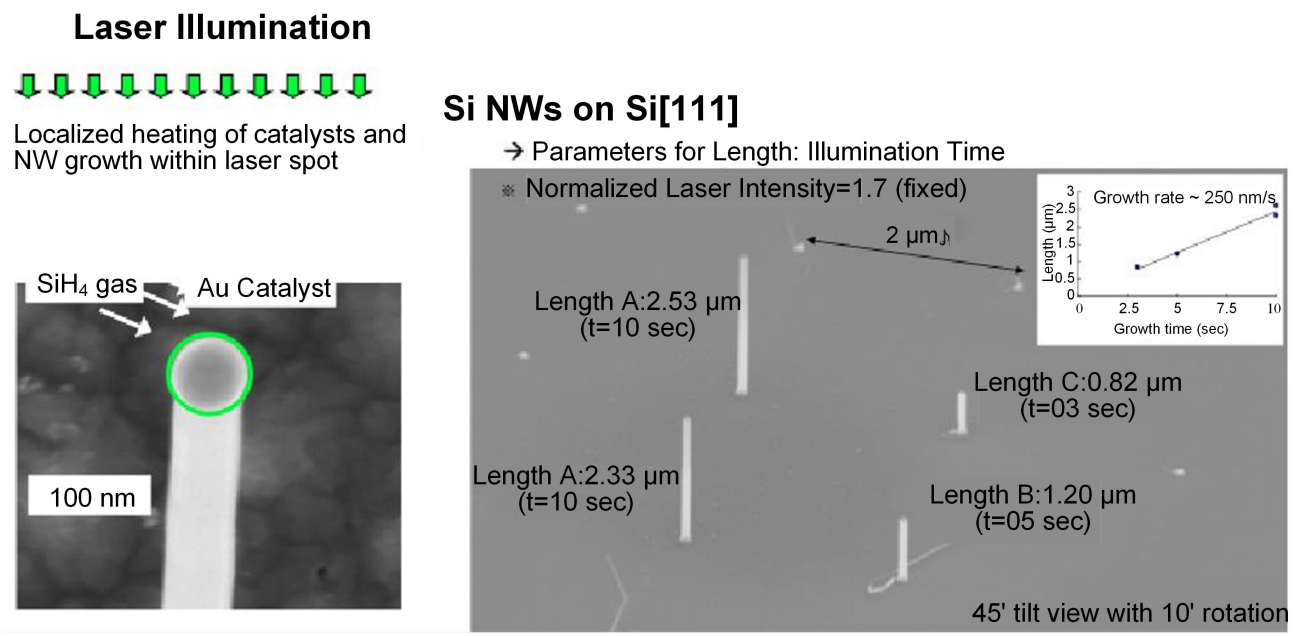

Figure 5. The left scanning electron microscopy (SEM) image depicts NW growth from Si atoms produced by the dissociated silane (SiH4) gas diffuse through the molten eutectic Au+Si catalyst towards the growing NW stem. The right picture depicts localized NW growth from Au NPs deposited by e-beam lithography on a 2 mm crystalline c-Si film on a fused Si wafer. Tightly focused continuous wave (CW) laser radiation at a visible wavelength (=543 nm) addresses each catalyst separately and drives homoepitaxial Si NW growth. The laser beam propagates through the transparent substrate to indirectly heat the catalyst. The length of the NWs is precisely regulated by the duration of the laser illumination.

(and hence multibandgap) semiconductor NW direct growth has been demonstrated on a single platform [81]. The reaction size can be tailored depending on the specific target application by regulating the laser power or by temporally/spatially modulating the laser irradiation. Arbitrary patterning of single element or compound NWs can be achieved on demand simply by switching the precursor gases.

A critical difference is identified in the growth time resolution as the furnace growth was ∼15 s. The relatively lower activation energy in laser-assisted growth is partly attributed to the difference in time resolution. However, localized CVD or growth by confined laser spot is advantageous in driving three-dimensional gas transport over a smaller reaction zone (CVD gas delivery and exchange of reaction byproducts such as hydrogen) versus 1D transport in wider reaction area cases [82]. Due to competing solid–liquid and vapor–liquid interfacial energy effects, the catalyst size affects SiNW growth kinetics and, therefore, the diameter and growth rate. In contrast to conventional furnace experiments that are of limited temporal resolution, regulating the duration of the laser illumination can precisely control the laser-driven NW growth [83]. Energy filtered transmission electron microscopy-based chemical mapping was employed to investigate the commencement of the laser-driven nucleation process (figure 6). In the regime of rapid and sustained growth, nucleation occurs in the time range of 10–100 ms depending on the catalyst diameter and growth temperature. The precise measurements of nucleation times elucidate the early stage behavior of catalyzed growth and reveal that the activation energy for the NW nucleation diminishes as the catalyst size is reduced. In a more general point of view, the laser heating methodology provides useful clues to a wide range of phenomena spanning from synthesis to phase change of nanomaterials.

The highly controlled spatial and temporal laser irradiation distribution enabled growth of discrete semiconductor NWs having precisely tunable dimensions on heteroepitaxial substrates [84]. Figure 7 shows VLS growth of vertical germanium nanowires (GeNWs) with deliberately varying shapes on a single Si(111) substrate by controlling the laser power (i.e. growth temperature) and illumination time. The irregular cross-sectional shape obtained at high temperatures was due to the anisotropy induced by the crystallographic orientation. Despite the lack of buffer layers to mitigate the lattice mismatch, the quality of the interface between the nanowire root and the substrate is excellent.

2.2. NSOM enabled selective nanowire growth

Highly selective growth of single SiNWs was achieved by means of an optical near-field technique [85]. Supportive, indirect heating of the catalyst provided to the underlying substrate via far-field laser irradiation lowered the level of direct near-field illumination onto the catalyst and also sustained the nanometer-scale heat source confinement. The actual exposure of the direct illumination beam on the catalyst was limited to the early stage of the growth and was followed by heat conduction to the catalyst through the nanowire stem. Damage-free, nanoscale spatial selectivity under the reactant gas was possible using a dielectric atomic force microscopy (AFM) tip. The optical near-field laser radiation was applied

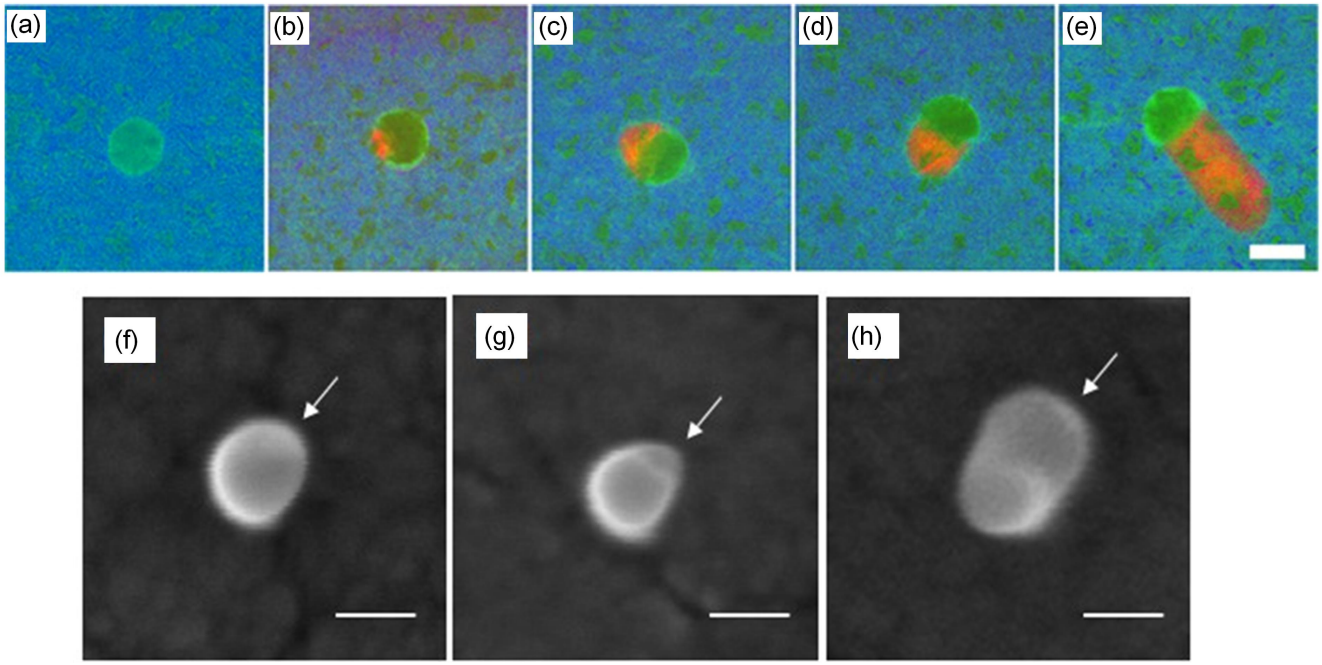

Figure 6. (a)–(e) Composite chemical maps for various growth times: (a) just prior to nucleation at 8 ms, (b) just after nucleation at 10 ms, (c) 40, (d) 80, and (e) 400 for 50 nm AuNP catalysts. Laser power was fixed at 7.5 mW (calibrated growth temperature of 918 K) and a partial pressure of SiH_4 maintained at 6 Torr with a flow rate of 600 sccm. The scale bar is 50 nm. (f)–(h) SEM images showing early stage growth behavior of SiNW: (f) just after nucleation at 10 ms, (g) 20 ms, and (h) 100 ms for 50 nm AuNP catalysts. The laser power was fixed at 7.5 mW (calibrated growth temperature of 918 K) and a partial pressure of SiH_4 maintained at 6 Torr. The scale bar is 50 nm. Reprinted from [83], with the permission of AIP Publishing.

on a single selected Au nanocatalyst in order to initiate nucleation and then drive the subsequent SiNW growth, as shown in figure 8(a). Figure 8(b) shows a scanning electron microscope image of discrete SiNWs selectively grown among randomly distributed Au nanocatalysts while the neighboring catalysts remained intact. Far-field indirect illumination was first provided onto the film, inducing no evident reaction within the heat-affected zone. Following a temporal delay, near-field direct illumination was superimposed onto the far-field radiation providing the impetus for the nanowire growth. The near-field illumination can induce an extra temperature increase in a AuNP at the very early growth stage when the AuNP is still under direct near-field illumination. The directionality of the NW could be improved by placing an electrically biased AFM tip over the catalyst during the laser-induced growth process [86].

3. Laser processing of atomic layered films

3.1. Localized doping

Two-dimensional (2D) transition metal dichalcogenide (TMDC) semiconductors with the general chemical formula of MX_2 (M = Mo, W; X = S, Se, Te) have attracted much interest due to their finite direct band gaps, rich excitonic dynamics, and valley polarization (valleytronics) associated with the broken inversion symmetry. These layered semiconductors, composed of vertically stacked layers held together by van der Waals interactions, are emerging as alternatives to Si-based electronics. The TMDC devices exhibit exceptional characteristics that are particularly suitable for next generation optoelectronic and electronic device applications [87–89]. They are excellent candidate materials for transistors [90–92], photodetectors [93, 94], electroluminescent devices [95], and sensors [96]. Despite the potential in electronics and optoelectronics, reliable and stable processing methods are needed for transition to practical applications [97]. More specifically, controlled doping of semiconductors is vital for integration into devices. However, previous efforts have mostly focused on doping TMDCs by means of charge transfer from adsorbed molecules [98], electrostatic [99] or physisorption gating [100], defect engineering [101], and substitutional doping during growth [102]. Site-specific doping with precise doping level control becomes essential, especially for nanoscale devices using ultrathin TMDCs in order to minimize random dopant fluctuation and ensure device performance reproducibility. A versatile method was reported for widely tunable, site-specific doping of ultrathin TMDCs (molybdenum disulfide (MoS_2) and tungsten diselenide (WSe_2)) through focused laser irradiation in a phosphine environment [103]. A schematic diagram of the laser-assisted doping process is shown in figure 9(a).

The laser serves two major functions: (i) creation of chalcogen vacancies in the TMDC materials and (ii) simultaneous dissociation of the dopant molecules. The released dopant molecules were incorporated into the vacancy sites. The phosphine (PH_3) doping of Si has been extensively studied, both experimentally and through theoretical modeling

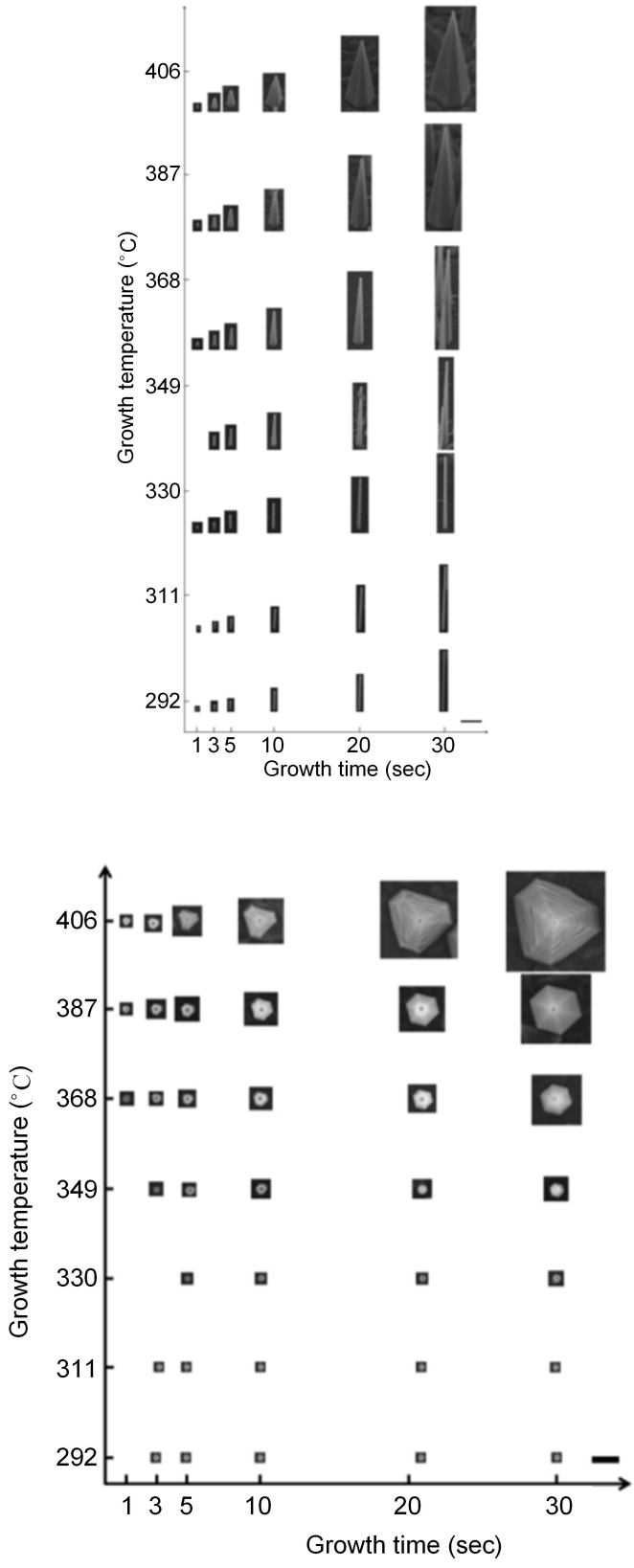

Figure 7. (Top) Field-emission scanning electron microscopy (FE-SEM) images at a 45° tilted angle of vertically grown GeNWs on Si(111). All NWs were grown on a single 4 μm thick c-Si bonded on quartz. The growth temperature ranged from 292 °C to 406 °C and the growth time from 1 to 20 s. The scale bar is 500 nm. (Bottom) Planar view images of vertically grown GeNWs on Si(111). The growth temperature ranged from 311 °C to 406 °C and the growth time from 1 to 30 s. The scale bar is 50 nm. Reprinted with permission from [84]. Copyright (2013) American Chemical Society.

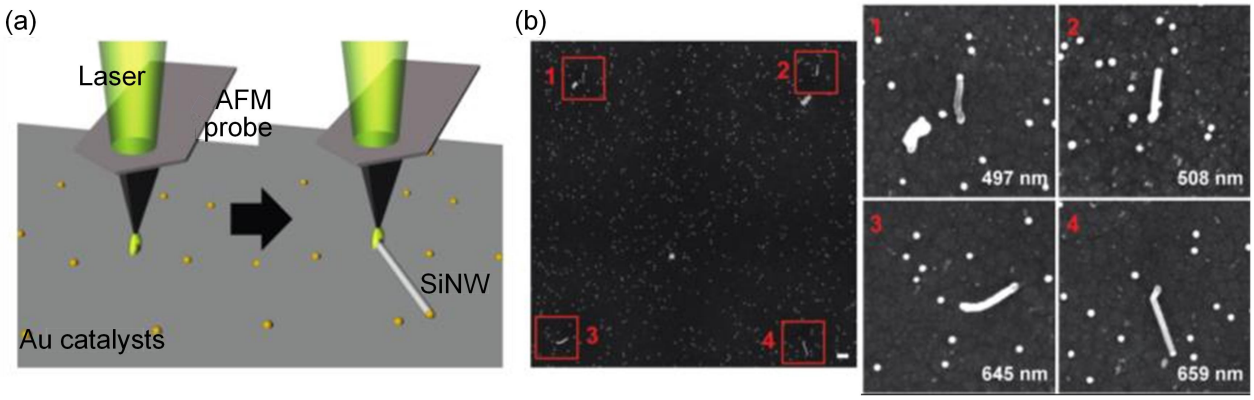

Figure 8. Highly selective growth of single SiNWs by near-field direct illumination over the AuNP, aided by supportive film heating by far-field indirect illumination. (a) Single catalysts were selected from randomly distributed AuNPs via the AFM mapping process for growth into a SiNW. Length control was implemented by adjusting the near-field laser irradiation power. (b) Each of two single NWs on top (1), (2) and at bottom (3), (4) were individually grown with 1.5 and 2.0 mW in laser input power for 5 s, respectively. The corresponding axial lengths were 503 (1), (2) and 652 nm (3), (4) on average. The scale bar is 500 nm. Reproduced from [85] (2014). With permission of Springer.

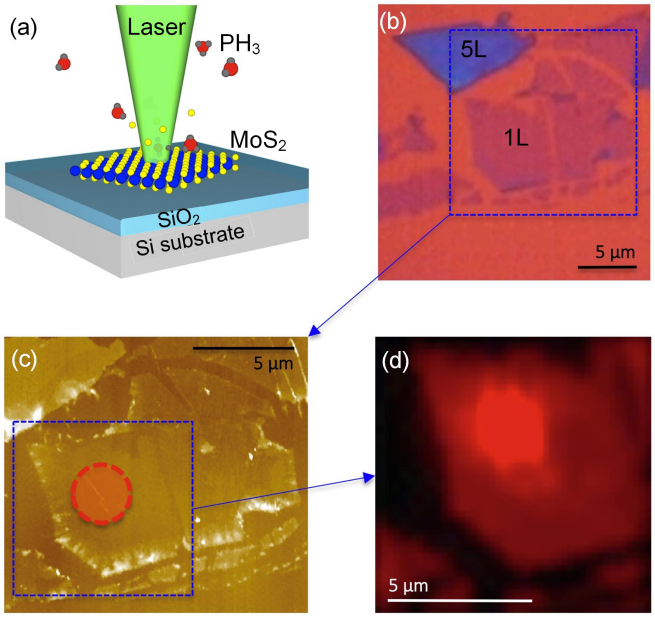

Figure 9. (a) Schematic diagram of the laser-assisted doping method. (b) Optical image of as-prepared monolayer MoS_2 on SiO_2/Si substrates. (c) Atomic force microscopy image of the zoomed area in (b). Its thickness is around 0.7 nm, in good agreement with the thickness of monolayer MoS_2. The circle in (c) is the laser spot area in the laser doping. (d) Photoluminescence (PL) mapping of the zoomed area in (c) that clearly shows the PL intensity enhancement of the laser-assisted doped area. [103] John Wiley & Sons.

[104]. Despite differences between Si and TMDCs, it is reasonable to adopt the substitutional doping mechanism. Considering that the dissociation temperature of TMDCs is in the range of 1200–1400 K, a laser power slightly below this range is enough to break the PH_3 molecules whose dissociation temperature is 685 K. Figure 9(b) shows an optical image of a mechanically exfoliated monolayer and five-layer MoS_2 flakes. The monolayer MoS_2 flake in figure 9(c) was ~0.7 nm thick. The PL map shown in figure 9(d) was taken from the laser-irradiated region indicated in figure 9(c). The laser doping process did not cause detrimental structural damage to these TMDCs at the given conditions.

Previous studies have already achieved both n- and p-type doping by surface charge transfer mechanisms, mostly through chemical physisorption [105]. However, physisorption doping is unstable and decays almost completely within an hour [106] or is retained for longer periods only if the doping environment is maintained or protected [92]. Among the various doping methods, substitutional doping of foreign elements is an effective and stable doping strategy for TMDCs. Accordingly, the laser was used to create sulfur vacancies and locally heat up the material to crack the precursor molecules, enabling the substitution of sulfur with phosphorus. The laser-assisted doping was shown to be irreversible and stable, even after

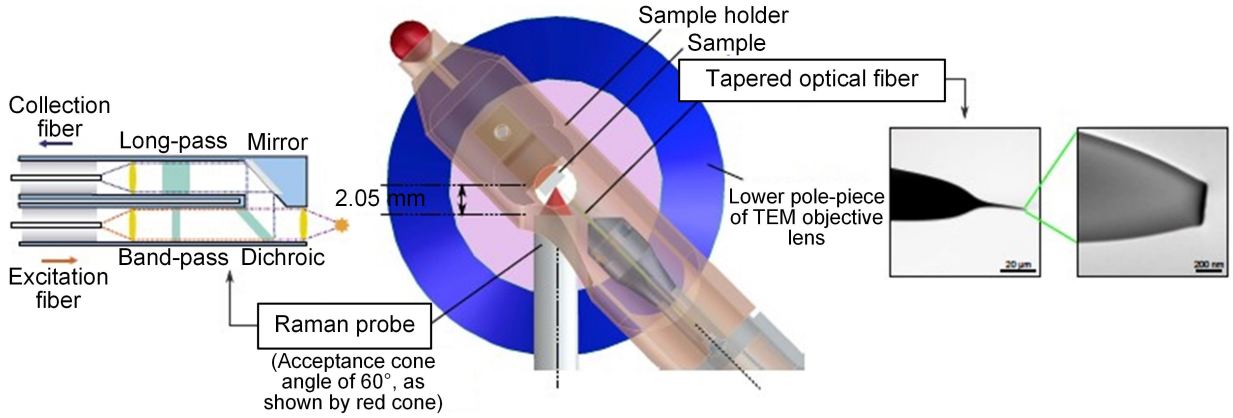

Figure 10. Layout of *in situ* Raman assembly in the sample chamber of the TEM (middle), schematic of Raman probe (left), and TEM images of tapered optical fiber (right). Reprinted from [115], Copyright (2017), with permission from Elsevier.

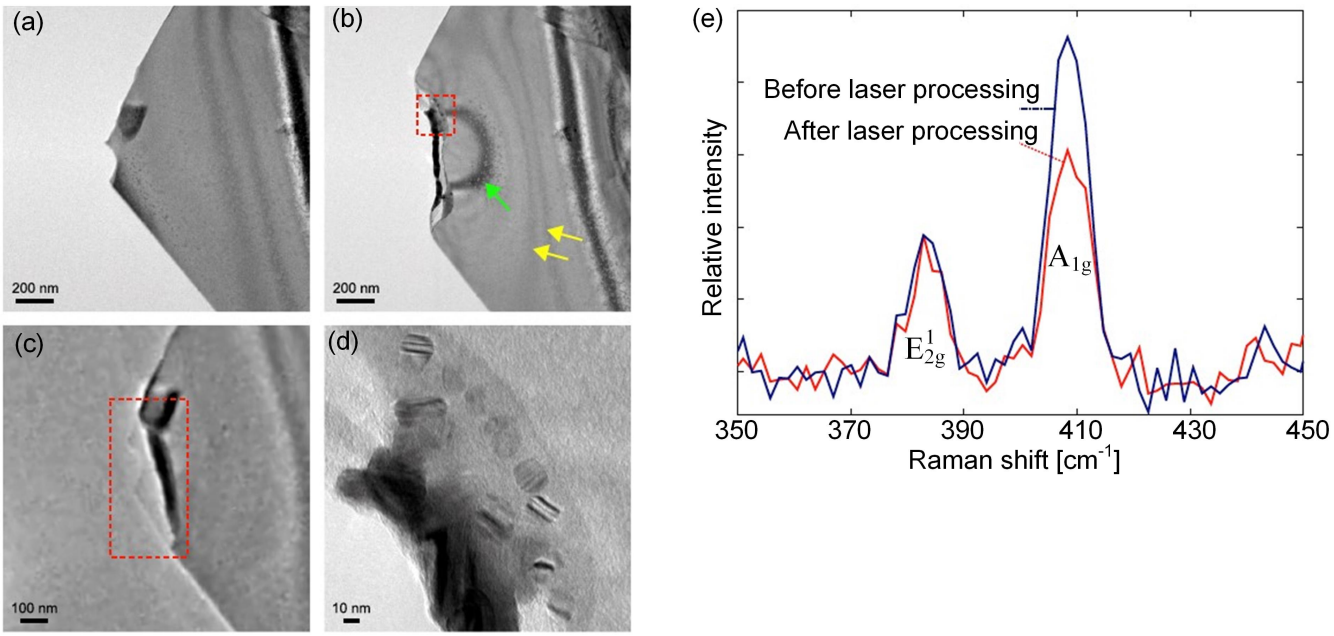

Figure 11. Bright-field TEM of MoS_2 flake (a) before and (b) after pulsed laser ablation. (c) Bright-field TEM snapshot from movie of the MoS_2 flake acquired during laser processing. (d) Higher magnification view of (b) showing spherical crystallites formed as a result of the pulsed laser processing. (e) Raman spectra of MoS_2 flake acquired before (blue) and after (red) laser processing, normalized to the *Eg* 21 peak and background subtracted. Reprinted from [115], Copyright (2017), with permission from Elsevier.

exposure in air for a month. In parallel to strong modification of the luminescent properties, the laser-assisted doping also drastically affected the electrical properties of the ultrathin TMDCs. This was investigated using field-effect transistor devices incorporating the locally doped TMDC layers as current channels.

This approach effectively introduced electronically active phosphorus atoms into the TMDCs. The precise level, temporal, and spatial control of the doping was achieved by varying the laser irradiation power and time, demonstrating wide tunability and high site selectivity. Future investigation on the choice of dopant, the dopant concentration, and the contact engineering should be conducted. The high stability and effectiveness of the laser-assisted doping method combined with the site selectivity and tunability demonstrated here may open a new avenue for functionalizing TMDCs for customized nanodevice applications.

Irradiation with a single continuous laser beam of Gaussian profile induces spatially nonuniform doping and, therefore, limits the potential of laser processing of TMDCs as a well-controlled tool for a wider range of applications. Advanced laser configuration is, therefore, required for decoupling the fundamental phenomena associated with the doping mechanism: (1) the dissociation of dopant molecules to provide dopant radicals, and (2) the laser treatment and ensuing structural modification on the TMDCs. These can be separately controlled via a dual laser beam configuration combining different pulse lengths and wavelengths. Furthermore, the dopant gas for laser doping can

be selected according to the desired p- or n-type doping effect. This approach represents a new concept for fabricating PN junctions on 2D materials, offering distinct advantages with respect to reducing the process time and minimizing random fluctuation of doping. To further expand the potential of TMDCs towards novel optoelectronic devices, bandgap tuning by laser alloying is a promising candidate and will be achieved by introducing atoms of another chalcogen (S, Se, and Te). Local replacement of Se by S atoms in TMDCs was demonstrated via a laser-assisted chemical modification process [107]. Furthermore, laser-induced selective decoration of few- and multilayer MoS_2 has been demonstrated with silver (Ag) NPs via the photo-excitation of the semiconductor material exposed to silver nitrate ($AgNO_3$) solution [108]. This route enables control of p-type doping by varying the laser irradiation time.

3.2. *In situ* observation of laser processing of MoS_2 layers

The unique and highly promising characteristics of TMDCs depend on their thickness, which is typically in ultrathin format of a few layers or monolayers. Monolayer MoS_2 has a direct bandgap of ~1.85 eV instead of the indirect bandgap of 1.2 eV for the bulk counterpart. Thus, control of the TMDC layer thickness in arbitrary patterns should add flexibility to fully explore their exotic properties and push forward potential applications. However, TMDC few or monolayer flakes that are typically exfoliated from bulk crystals can have high crystallinity but rely on the spatially random van der Waals force between flakes and substrate resulting in uncontrollable thickness and shape. A tightly focused continuous-wave laser beam was utilized to thin MoS_2 down to a single layer [109]. The semiconducting properties of the thinned layers were found to resemble the properties of pristine MoS_2 single layers. Evidently, the laser light absorption into the semiconducting material changes dynamically during the thinning process. Moreover, the thermal conductivity of TMDC materials varies with the number of layers and is influenced by the backing substrate [110]. Consequently, the laser thinning represents a self-regulated process. A photochemical variance of the laser thinning process was presented in [111], utilizing adsorbed H_2O molecules on molybdenum (IV) telluride ($MoTe_2$) layers from the humidity present in the atmosphere to effect thinning under very low laser powers. Laser excitation at ultralow laser power in vacuum was shown to induce irreversible changes in the optical properties of TMDC materials [112]. An *in situ* study of void formation upon CW laser irradiation, with the assistance of temporal Raman evolution, yielded an empirical formula relating void size to laser power and exposure time [113]. Ultrafast laser-based thinning of MoS_2 through a two-photon absorption process was reported [114]. The interaction of laser radiation with TMDC material involves complex nanoscale physicochemical phenomena and, therefore, calls for further investigation. An *in situ* Raman instrument extending the capability of the TEM apparatus described in section 1.1 was utilized to quantitatively probe the laser thinning process of a MoS_2 flake (figures 10 and 11). Further studies are needed to understand the precise mechanism of the laser interaction and modification of these exotic materials and push their applications, including in optoelectronics, flexible electronics, and sensors.

Acknowledgments

The research was performed at the Laser Thermal Laboratory by Drs David J Hwang, Sang-gil Ryu, Eunpa Kim, Jung Bin In, and the current students, Letian Wang, Yoonsoo Rho and Matthew Eliceiri. Professors Andrew M Minor, Junqiao Wu, Oscar D Dubon, Drs Bin Xiang, Frances I Allen, and Changhyun Ko of UCB Materials Science and Engineering, and Dr Carlo Carraro of UCB Chem. Engineering contributed to the work. The research was supported by DARPA/MTO under TBN grant N66001-08-1-2041, the US Department of Energy SBIR grant (DE-FG02-07ER84813), Samsung GRO, and NSF CMMI-1363392. The *in situ* experiments were performed at the National Center for Electron Microscopy at the Lawrence Berkeley National Laboratory, which is supported by the Office of Science, Office of Basic Energy Sciences, Scientific User Facilities Division, of the US Department of Energy under Contract No. DE-AC02-05CH11231. The laser-induced nanowire growth and doping was conducted on the LACVD apparatus in the UC Berkeley Marvell Nanofabrication Laboratory.

References

[1] Park I, Ko S H, Pan H, Grigoropoulos C P, Pisano A P, Fréchet J M J, Lee E S and Jeong J-H 2008 Nanoscale patterning and electronics on flexible substrate by direct nanoimprinting of metallic nanoparticles *Adv. Mater.* **20** 489–96

[2] Im J S and Kim H J 1994 On the super lateral growth phenomenon observed in excimer laser-induced crystallization of thin Si films *Appl. Phys. Lett.* **64** 2303–5

[3] Brotherton S D 1995 Polycrystalline silicon thin-film transistors *Semicond. Sci. Technol.* **10** 721–38

[4] Andra G, Bergmann J, Falk F and Ose E 1999 *In-situ* diagnostics for preparation of laser crystallized silicon films on glass for solar cells *Thin Solid Films* **337** 98–100

[5] Sposili R S and Im J S 1996 Sequential lateral solidification of thin silicon films on SiO_2 *Appl. Phys. Lett.* **69** 2864–6

[6] Hatano M, Moon S, Lee M, Suzuki K and Grigoropoulos C P 2000 Excimer laser-induced temperature field in melting and resolidification of silicon thin films *J. Appl. Phys.* **87** 36–43

[7] van der Wilt P C, van Dijk B D, Bertens G J, Ishihara R and Beenakker C I M 2001 Formation of location-controlled crystalline islands using substrate-embedded seeds in excimer-laser crystallization of silicon films *Appl. Phys. Lett.* **79** 1819–21

[8] Zhang J, Trifunovic M, van der Zwan M, Takagishi H, Kawajiri R, Shimoda T, Beenakker C I M and Ishihara R 2013 Single-grain Si thin-film transistors on flexible polyimide substrate fabricated from doctor-blade coated liquid-Si *Appl. Phys. Lett.* **102** 243502

[9] Hu S, Leu P W, Marshall A F and McIntyre P C 2009 Single-crystal germanium layers grown on silicon by nanowire seeding *Nat. Nanotechnol.* **4** 649–53

[10] Taheri M L, Reed B W, Lagrange T B and Browning N D 2008 *In situ* laser synthesis of si nanowires in the dynamic TEM *Small* **4** 2187–90

[11] Taheri M L, Lagrange T, Reed B W, Armstrong M R, Campbell G H, Dehope W J, Kim J S, King W E, Masiel D J and Browning N D 2009 Laser-based *in situ* techniques: novel methods for generating extreme conditions in TEM samples *Microsc. Res. Tech.* **72** 122–30

[12] Chimmalgi A, Hwang D J and Grigoropoulos C P 2005 Nanoscale rapid melting and crystallization of semiconductor thin films *Nano Lett.* **5** 1924–30

[13] Arora H, Du P, Tan K W, Hyun J K, Grazul J, Xin H L, Muller D A, Thompson M O and Wiesner U 2010 Block copolymer self-assembly-directed single-crystal homo- and heteroepitaxial nanostructures *Science* **330** 214–9

[14] Xiang B, Hwang D J, In J-B, Ryu S-G, Yoo J-H, Dubon O D, Minor A M and Grigoropoulos C P 2012 *In-situ* TEM near field optical probing of nanoscale silicon crystallization *Nano Lett.* **12** 2524–9

[15] Hwang D J, Grigoropoulos C P, Yoo J and Russo R E 2006 Optical near field ablation-induced plasma characteristics *Appl. Phys. Lett.* **89** 254101

[16] Taheri M L, McGowan S, Nikolova L, Evans J E, Teslich N, Lu J P, LaGrange T, Rosei F, Siwick B J and Browning N D 2010 *In situ* laser crystallization of amorphous silicon: controlled nanosecond studies in the dynamic transmission electron microscope *Appl. Phys. Lett.* **97** 032102

[17] Nikolova L, LaGrange T, Reed B W, Stern M J, Browning N D, Campbell G H, Kieffer J C, Siwick B J and Rosei F 2010 Nanocrystallization of amorphous germanium films observed with nanosecond temporal resolution *Appl. Phys. Lett.* **97** 203102

[18] Evans P V, Devaud G, Kelly T F and Kim Y K 1990 Solidification in highly undercooled Si and Ge droplets *Acta Metall. Mater.* **38** 719–28

[19] Leonard J P and Im J S 2001 Stochastic modeling of solid nucleation in supercooled liquids *Appl. Phys. Lett.* **78** 3454–8

[20] Leonard J P and Im J S 2000 Modeling solid nucleation and growth in supercooled liquid, in nucleation and growth processes in materials *Proc. Mater. Res. Soc.* **580** 233

[21] Skripov V P 1977 *Crystal Growth and Materials* ed E Kaldis and H J Scheel (Amsterdam: North-Holland) p 328

[22] Kisdarjono H, Voutsas A T and Solanki R J 2003 Three-dimensional simulation of rapid melting and resolidification of thin si films by excimer laser annealing *J. Appl. Phys.* **94** 4374–81

[23] Im J S, Gupta V V and Crowder M A 1998 On determining the relevance of athermal nucleation in rapidly quenched liquids *Appl. Phys. Lett.* **72** 662–4

[24] Shneidman V A 1999 Analytical description of 'athermal' nucleation and its relevance to rapidly quenched fluids *J. Appl. Phys.* **85** 1981–3

[25] Vanamu G, Datye A K and Zaidi S H 2006 Epitaxial growth of high-quality Ge films on nanostructured silicon substrates *Appl. Phys. Lett.* **88** 204104

[26] In J B, Xiang B, Ryu S-G, Kim E, Yoo J-H, Dubon O, Minor A M and Grigoropoulos C P 2014 Generation of single-crystalline domain in nano-scale silicon pillars by near field short pulsed laser *Appl. Phys.* A **114** 277–85

[27] Leung B, Song J, Zhang Y and Han J 2013 Evolutionary selection growth: towards template-insensitive preparation of single-crystal layers *Adv. Mater.* **25** 1285–9

[28] Shipway A N, Katz E and Willner I 2000 Nanoparticle arrays on surfaces for electronic, optical, and sensor applications *ChemPhysChem* **1** 18–52

[29] Cavallini M, Biscarini F, Gomez-Segura J, Ruiz D and Veciana J 2003 Multiple length scale patterning of single-molecule magnets *Nano Lett.* **3** 1527–30

[30] Somorjai G A, York R L, Butcher D and Park J Y 2007 The evolution of model catalytic systems, studies of structure, bonding and dynamics from single crystal metal surfaces to nanoparticles, and from low pressure ($<10^{-3}$ Torr) to high pressure ($>10^{-3}$ Torr) to liquid interfaces *Phys. Chem. Chem. Phys.* **9** 3500–13

[31] Stewart M E, Anderton C R, Thompson L B, Maria J, Gray S K, Rogers J A and Nuzzo R G 2008 Nanostructured plasmonic sensors *Chem. Rev.* **108** 494–521

[32] Kuznetsov A I, Miroshnichenko A E, Brongersma M L, Kivshar Y S and Luk'yanchuk B 2016 Optically resonant dielectric nanostructures *Science* **354** 6314

[33] Jahani S and Jacob Z 2016 All-dielectric metamaterials *Nat. Nanotechnol.* **11** 23–36

[34] Cui P, Seo S, Lee J, Wang L, Lee E, Min M and Lee H 2011 Nonvolatile memory device using gold nanoparticles covalently bound to reduced graphene oxide *ACS Nano* **5** 6826–33

[35] Tsoukalas D 2009 From silicon to organic nanoparticle memory devices *Phil. Trans* A **367** 4169–79

[36] Zijlstra P, Chon J W M and Gu M 2009 Five-dimensional optical recording mediated by surface plasmons in gold nanorods *Nature* **459** 410–3

[37] Wu H *et al* 2012 Stable cycling of double-walled silicon nanotube battery anodes through solid-electrolyte interphase control *Nat. Nanotechnol.* **7** 310–5

[38] Fowlkes J D, Roberts N A, Wu Y, Diez J A, González A G, Hartnett C, Mahady K, Afkhami S, Kondic L and Rack P D 2014 Hierarchical nanoparticle ensembles synthesized by liquid phase directed self-assembly *Nano Lett.* **14** 774–82

[39] Fowlkes J D, Kondic L, Diez J, Wu Y and Rack P D 2011 Self-assembly *versus* directed assembly of nanoparticles via pulsed laser induced dewetting of patterned metal films *Nano Lett.* **11** 2478–85

[40] Wood T *et al* 2017 All-dielectric color filters using SiGe-based mie resonator arrays *ACS Photonics* **4** 873–83

[41] Ye J and Thompson C V 2011 Templated solid-state dewetting to controllably produce complex patterns *Adv. Mater.* **23** 1567–71

[42] Cui Y, Björk M T, Liddle J A, Sönnichsen C, Boussert B and Alivisatos A P 2004 Integration of colloidal nanocrystals into lithographically patterned devices *Nano Lett.* **4** 1093–8

[43] Flauraud V, Mastrangeli M, Bernasconi G D, Butet J, Alexander D T L, Shahrabi E, Martin O J F and Brugger J 2017 Nanoscale topographical control of capillary assembly of nanoparticles *Nat. Nanotechnol.* **12** 73–80

[44] Zhu X, Vannahme C, Højlund-Nielsen E, Mortensen N A and Kristensen A 2016 Plasmonic colour laser printing *Nat. Nanotechnol.* **11** 325–9

[45] Zhu X, Yan W, Levy U, Mortensen N A and Kristensen A 2017 Resonant laser printing of structural colors on high-index dielectric metasurfaces *Sci. Adv.* **3** e1602487

[46] Chen Y, Duan X, Matuschek M, Zhou Y, Neubrech F, Duan H and Liu N 2017 Dynamic color displays using stepwise cavity resonators *Nano Lett.* **17** 5555–60

[47] Duan X, Kamin S and Liu N 2017 Dynamic plasmonic colour display *Nat. Commun.* **8** 1–9

[48] Wang X, Kuchmizhak A, Storozhenko D, Makarov S V and Juodkazis S 2017 Single-step laser plasmonic coloration of metal films *ACS Appl. Mater. Interfaces* **10** 1422–7

[49] Wuttig M and Yamada N 2007 Phase-change materials for rewriteable data storage *Nat. Mater.* **6** 824–32

[50] Gu M and Li X 2010 The road to multi-dimensional bit-by-bit optical data storage *Opt. Photonics News* **21** 28–33

[51] Wang Q, Rogers E T F, Gholipour B, Wang C-M, Yuan G, Teng J and Zheludev N I 2015 Optically reconfigurable metasurfaces and photonic devices based on phase change materials *Nat. Photonics* **10** 60–5

[52] Tittl A, Michel A K U, Schäferling M, Yin X, Gholipour B, Cui L, Wuttig M, Taubner T, Neubrech F and Giessen H 2015 A switchable mid-infrared plasmonic perfect absorber with multispectral thermal imaging capability *Adv. Mater.* **27** 4597–603

[53] Michel A-K U, Chigrin D N, Maß T W W, Schönauer K, Salinga M, Wuttig M and Taubner T 2013 Using low-loss phase-change materials for mid-infrared antenna resonance tuning *Nano Lett.* **13** 3470–5

[54] Hong S, Lee H, Yeo J and Ko S H 2016 Digital selective laser methods for nanomaterials: from synthesis to processing *Nano Today* **11** 547–64

[55] Sygletou M, Petridis C, Kymakis E and Stratakis E 2017 Advanced photonic processes for photovoltaic and energy storage systems *Adv. Mater.* **29** 170035

[56] Makarov S V, Zalogina A S, Tajik M, Zuev D A, Rybin M V, Kuchmizhak A A, Juodkazis S and Kivshar Y 2017 Light-induced tuning and reconfiguration of nanophotonic structures *Laser Photonics Rev.* **11** 1–25

[57] Zywietz U, Evlyukhin A B, Reinhardt C and Chichkov B N 2014 Laser printing of silicon nanoparticles with resonant optical electric and magnetic responses *Nat. Commun.* **5** 3402

[58] Wang L *et al* 2018 Programming nanoparticles in multiscale: optically modulated assembly and phase switching of silicon nanoparticle array *ACS Nano* **12** 2231–41

[59] Dong K *et al* 2017 A lithography-free and field-programmable photonic metacanvas *Adv. Mater.* **30** 1703878

[60] Zhao W, Jiang H, Liu B, Jiang Y, Tang C and Li J 2015 Fano resonance based optical modulator reaching 85% modulation depth *Appl. Phys. Lett.* **107** 171109

[61] Zhao W, Leng X and Jiang Y 2015 Fano resonance in all-dielectric binary nanodisk array realizing optical filter with efficient linewidth tuning *Opt. Express* **23** 6858

[62] Huang Z, Wang J, Liu Z, Xu G, Fan Y, Zhong H, Cao B, Wang C and Xu K 2015 Strong-field-enhanced spectroscopy in silicon nanoparticle electric and magnetic dipole resonance near a metal surface *J. Phys. Chem.* C **119** 28127–35

[63] Tian B, Zheng X, Kempa T J, Fang Y, Yu N, Yu G, Huang J and Lieber C M 2007 Coaxial silicon nanowires as solar cells and nanoelectronic power sources *Nature* **449** 885–U8

[64] Kempa T J, Tian B Z, Kim D R, Hu J S, Zheng X L and Lieber C M 2008 Single and tandem axial p–i–n nanowire photovoltaic devices *Nano Lett.* **8** 3456–60

[65] Chan C K, Peng H, Liu G, McIlwrath K, Zhang X F, Huggins R A and Cui Y 2008 High-performance lithium battery anodes using silicon nanowires *Nat. Nanotechnol.* **3** 31–5

[66] Aricò A S, Bruce P, Scrosati B, Tarascon J M and van Schalkwijk W 2005 Nanostructured materials for advanced energy conversion and storage devices *Nat. Mater.* **4** 366–77

[67] Pauzauskie P J and Yang P 2006 Nanowire photonics *Mater. Today* **9** 36–45

[68] Yan R, Gargas D and Yang P 2009 Nanowire photonics *Nat. Photon.* **3** 569–76

[69] Qing Q, Pal S K, Tian B, Duan X, Timko B P, Cohen-Karni T, Murthy V N and Lieber C M 2010 Nanowire transistor arrays for mapping neural circuits in acute brain slices *Proc. Natl Acad. Sci.* **107** 1882–7

[70] Zheng G, Patolsky F, Cui Y, Wang W U and Lieber C M 2005 Multiplexed electrical detection of cancer markers with nanowire sensor arrays *Nat. Biotechnol.* **23** 1294–301

[71] Pauzauskie P J, Radenovic A, Trepagnier E, Shroff H, Yang P and Liphardt J 2006 Optical trapping and integration of semiconductor nanowire assemblies in water *Nat. Mater.* **5** 97–101

[72] Jamshidi A, Pauzauskie P J, Schuck P J, Ohta A T, Chiou P Y, Chou J, Yang P and Wu M C 2008 Dynamic manipulation and separation of individual semiconducting and metallic nanowires *Nat. Photon.* **2** 86–9

[73] Boyd D A, Greengard L, Brongersma M, El-Naggar M Y and Goodwin D G 2006 Plasmon-assisted chemical vapor deposition *Nano Lett.* **6** 2592–6

[74] Cao L, Barsic D N, Guichard A R and Brongersma M L 2007 Plasmon-assisted local temperature control to pattern individual semiconductor nanowires and carbon nanotubes *Nano Lett.* **7** 3523–7

[75] Hung W H, Hsu I K, Bushmaker A, Kumar R, Theiss J and Cronin S B 2008 Laser directed growth of carbon-based nanostructures by plasmon resonant chemical vapor deposition *Nano Lett.* **8** 3278–82

[76] Chen Z, Zhu F, Wei Y, Jiang K, Liu L and Fan S 2008 Scanning focused laser activation of carbon nanotube cathodes for field emission flat panel displays *Nanotechnology* **19** 135703

[77] Bäuerle D, Irsigler P, Leyendecker G, Noll H and Wagner D 1982 Ar^+ laser-induced chemical vapor-deposition of Si from SiH_4 *Appl. Phys. Lett.* **40** 819–21

[78] Bäuerle D 2011 *Laser Processing and Chemistry* 4th edn (Heidelberg: Springer)

[79] Kikkawa J, Ohno Y and Takeda S 2005 Growth rate of silicon nanowires *Appl. Phys. Lett.* **86** 123109

[80] Hwang D J, Ryu S-G and Grigoropoulos C P 2011 Multi-parametric growth of silicon nanowires in a single platform by laser-induced localized heat sources *Nanotechnology* **22** 385303

[81] Hwang D J, Ryu S-G, Kim E, Grigoropoulos C P and Carraro C 2011 On demand-direct synthesis of Si and Ge nanowires on a single platform by focused laser illumination *Appl. Phys. Lett.* **99** 123109

[82] Kotecki D E and Herman I P 1988 A real-time monte-carlo simulation of thin film nucleation in localized laser chemical vapor deposition *J. Appl. Phys.* **64** 4920–42

[83] Ryu S-G, Kim E, Allen F I, Hwang D J, Minor A M and Grigoropoulos C P 2016 Incubation behavior of silicon nanowire growth investigated by laser-assisted rapid heating *Appl. Phys. Lett.* **109** 073106

[84] Ryu S-G, Yoo J-H, Kim E, Hwang D J, Xiang B, Dubon O D, Minor A M and Grigoropoulos C P 2013 On Demand shape-selective integration of individual vertical germanium nanowires on a Si(111) substrate via laser-localized heating *ACS Nano* **7** 2090–8

[85] Ryu S-G, Hwang D J, Kim E and Grigoropoulos C P 2014 Tip-based nanoscale selective growth of discrete silicon nanowires by near field laser illumination *Appl. Phys.* A **116** 51–8

[86] Ryu S-G, Kim E, Hwang D J and Grigoropoulos C P 2015 Selective and directed growth of silicon nanowires by tip-enhanced local electric field *Appl. Phys.* A **121** 255–60

[87] Wang Q H, Kalantar-Zadeh K, Kis A, Coleman J N and Strano M S 2012 Electronics and optoelectronics of two-dimensional transition metal dichalcogenides *Nat. Nanotechnol.* **7** 699–712

[88] Jariwala D, Sangwan V K, Lauhon L J, Marks T J and Hersam M C 2014 Emerging device applications for semiconducting two-dimensional transition metal dichalcogenides *ACS Nano* **8** 1102–20

[89] Ganatra R and Zhang Q 2014 Few-layer MoS_2: a promising layered semiconductor *ACS Nano* **8** 4074–9

[90] Radisavljevic B, Radenovic A, Brivio J, Giacometti V and Kis A 2011 Single-layer MoS_2 transistors *Nat. Nanotechnol.* **6** 147–50

[91] Wang H, Yu L L, Lee Y H, Shi Y M, Hsu A, Chin M L, Li L J, Dubey M, Kong J and Palacios T 2012 Integrated circuits based on bilayer MoS_2 transistors *Nano Lett.* **12** 4674–80

[92] Kim S *et al* 2012 High-mobility and low-power thin-film transistors based on multilayer MoS_2 crystals *Nat. Commun.* **3** 1011

[93] Lopez-Sanchez O, Lembke D, Kayci M, Radenovic A and Kis A 2013 Single-layer MoS_2 phototransistors, ultrasensitive photodetectors based on monolayer MoS_2 *Nat. Nanotechnol.* **8** 497–501

[94] Yin Z, Li H, Li H, Jiang L, Shi Y, Sun Y, Lu G, Zhang Q, Chen X and Zhang H 2012 Single-layer MoS_2 phototransistors *ACS Nano* **6** 74–80

[95] Ross J S *et al* 2014 Electrically tunable excitonic light-emitting diodes based on monolayer WSe_2 p–n junctions *Nat. Nanotechnol.* **9** 268–72

[96] Cho B *et al* 2015 Chemical sensing of 2D graphene/MoS_2 heterostructure device *ACS Appl. Mater. Interfaces* **7** 16775–80

[97] Butler S Z *et al* 2013 Progress, challenges, and opportunities in two-dimensional materials beyond graphene *ACS Nano* **7** 2898–926

[98] Tarasov A, Zhang S Y, Tsai M Y, Campbell P M, Graham S, Barlow S, Marder S R and Vogel E M 2015 Controlled doping of large-area trilayer MoS_2 with molecular reductants and oxidants *Adv. Mater.* **27** 1175–81

[99] Mak K F, He K L, Lee C, Lee G H, Hone J, Heinz T F and Shan J 2013 Tightly bound trions in monolayer MoS_2 *Nat. Mater.* **12** 207–11

[100] Tongay S, Zhou J, Ataca C, Liu J, Kang J S, Matthews T S, You L, Li J B, Grossman J C and Wu J Q 2013 Broad-range modulation of light emission in two-dimensional semiconductors by molecular physisorption gating *Nano Lett.* **13** 2831–6

[101] Nan H Y *et al* 2014 Strong photoluminescence enhancement of MoS_2 through defect engineering and oxygen bonding *ACS Nano* **8** 5738–45

[102] Suh J *et al* 2014 Doping against the native propensity of MoS_2: degenerate hole doping by cation substitution *Nano Lett.* **14** 6976–82

[103] Kim E *et al* 2016 Site selective doping of ultra-thin metal dichalcogenides by laser-assisted reaction *Adv. Mater.* **28** 341–6

[104] Wilson H F, Warschkow O, Marks N A, Curson N J, Schofield S R, Reusch T C G, Radny M W, Smith P V, McKenzie D R and Simmons M Y 2006 Thermal dissociation and desorption of PH3 on Si(001): a reinterpretation of spectroscopic data *Phys. Rev.* B **74** 195310

[105] Mouri S, Miyauchi Y and Matsuda K 2013 Tunable photoluminescence of monolayer MoS_2 via chemical doping *Nano Lett.* **13** 5944–8

[106] Zhao P D *et al* 2014 Air stable p-doping of WSe_2 by covalent functionalization *ACS Nano* **8** 10808–14

[107] Afaneh T, Sahoo P K, Nobrega I A P, Xin Y and Gutiérrez H R 2018 Laser-assisted chemical modification of monolayer transition metal dichalcogenides *Adv. Funct. Mater.* **28** 1802949

[108] Kim E *et al* 2108 Tuning the electrical and optical properties of MoS_2 by selective Ag photo-reduction *Appl. Phys. Lett.* **113** 013105

[109] Castellanos-Gomez A, Barkelid M, Goossens A M, Calado V E, van der Zant H S J and Steele G A Laser-thinning of MoS_2: on demand generation of a single-layer semiconductor *Nano Lett.* **12** 3187–92

[110] Malekpour H and Balandin A A 2017 Raman-based technique for measuring thermal conductivity of graphene and related materials *J. Raman Spectrosc.* **49** 106–20

[111] Nagareddy V K, Octon T J, Townsend N J, Russo S, Cracium M F and Wright D 2018 Humidity-controlled ultralow power layer-by-layer thinning, nanopatterning and bandgap engineering of $MoTe_2$ *Adv. Funct. Mater.* **28** 1804434

[112] Cadiz F *et al* 2016 Ultra-low power threshold for laser induced changes in optical properties of 2D molybdenum dichalcogenides *2D Mater.* **3** 045008

[113] Gu E, Wang Q, Zhang Y, Cong C, Hu L, Tian P, Liu R, Zhang S L and Qiu Z J 2017 A real-time raman spectroscopy study of the dynamics of laser-thinning of MoS_2 flakes to monolayers *AIP Adv.* **7** 125329

[114] Paradisanos I, Kymakis E, Fotakis C, Kioseoglou G and Stratakis E 2014 Intense femtosecond photoexcitation of bulk and monolayer MoS_2 *Appl. Phys. Lett.* **105** 041108

[115] Allen F I, Kim E, Andersen N C, Grigoropoulos C P and Minor A M 2017 *In situ* TEM Raman spectroscopy and laser-based materials modification *Ultramicroscopy* **178** 33–7